DMD Fast Forward. Published on April 4, 2011 as doi:10.1124/dmd.111.038315

In Vitro Metabolism of Irosustat, a Novel Steroid Sulphatase Inhibitor: Inter-Species Comparison, Metabolite Identification and Metabolic Enzyme Identification

Verònica Ventura, Josep Solà, Carles Celma, Concepción Peraire and Rosendo Obach

Ipsen Pharma, S.A. Department of Drug Metabolism and Pharmacokinetics, Sant Feliu de Llobregat, Barcelona, Spain.

DMD Fast Forward. Published on April 4, 2011 as DOI: 10.1124/dmd.111.038315
This article has not been copyedited and formatted. The final version may differ from this version.
DMD #38315

Running Title: *In Vitro* Metabolism of Irosustat

Corresponding Author:

Josep Solà (e-mail: josep.sola@ipsen.com)

Ipsen Pharma S.A. Crta. Laureà Miró, 395. 08980 Sant Feliu del Llobregat, Barcelona, Spain

Telephone: +34 93 685 81 00 / Fax: +34 93 685 10 53

Number of text pages: 45 (including references and tables)

Tables: 8

Figures: 4

References: 22

Abstract: 238 / 250

Introduction: 453 / 750

Discussion: 1478 / 1500

Nonstandard abbreviations used are: $Cl_{int,app}$ apparent intrinsic clearance; CYP, cytochrome P450; FMO, flavin-containing monooxygenase; HLM, human liver microsomes; HPLC, high-performance liquid chromatography; K_M, Michaelis Menten constant; LC-MS, liquid chromatography mass spectrometry; MS, mass spectrometry; NMR, nuclear magnetic resonance spectroscopy; SPE, solid phase extraction; STS, steroid sulphatase; SULT, sulfotransferase; UGT, UDP glucuronosyltransferase.

DMD Fast Forward. Published on April 4, 2011 as DOI: 10.1124/dmd.111.038315
This article has not been copyedited and formatted. The final version may differ from this version.

Abstract

Irosustat is a novel steroid sulphatase inhibitor for hormone-dependent cancer therapy. Its structure is a tricyclic coumarin-based sulphamate which undergoes de-sulphamoylation in aqueous solution yielding the sulphamoyl-free derivative, 667-Coumarin. The aim of the present work was to study the *in vitro* metabolism of Irosustat including its metabolic profile in liver microsomes and hepatocytes, the potential species differences, and the identification of the main metabolites and of the enzymes participating in its metabolism. Irosustat was extensively metabolized *in vitro,* showing similar metabolite profiles among rat, dog, monkey and humans (both sexes). In liver microsomes, the dog appeared as the species that metabolized Irosustat most similarly to humans. Marked differences were found between liver microsomes and hepatocytes, meaning that phase I and phase II enzymes contribute to Irosustat metabolism. Various mono-hydroxylated metabolites of Irosustat and of 667-Coumarin were found in liver microsomes, which mostly involved hydroxylations at the C8, C10 and C12 positions in the cycloheptane ring moiety. 667-Coumarin was formed by degradation but also by non-NADPH-dependent enzymatic hydrolysis, probably catalyzed by microsomal steroid sulphatase. The main metabolites formed by hepatocytes were glucuronide and sulphate conjugates of 667-Coumarin and of some of its mono-hydroxylated metabolites. The major P450 enzymes involved in the transformation of Irosustat were: CYP2C8, CYP2C9, CYP3A4/5 and CYP2E1. Moreover, various phase II enzymes (UGTs and SULTs) were capable of conjugating many of the metabolites of Irosustat and 667-Coumarin, however, the clinically relevant isoforms could not be elucidated.

DMD Fast Forward. Published on April 4, 2011 as DOI: 10.1124/dmd.111.038315
This article has not been copyedited and formatted. The final version may differ from this version.

Introduction

Irosustat, also known as BN83495, 667 COUMATE, or STX64, is an irreversible steroid sulphatase (STS) inhibitor for steroid hormone-dependent cancer therapy, and it is currently under clinical development by the Ipsen Group. STS enzyme is widely distributed throughout the body and regulates the formation of estrone and dehydroepiandrosterone from their corresponding sulphate conjugates. Both compounds can be further converted to estradiol and androstenediol, respectively, which are described to promote tumour growth (Reed et al., 2005; Foster, 2008). Irosustat exhibits potent STS inhibition both *in vitro,* showing an IC_{50} value of 8 nM in placental microsome preparations (Woo et al., 2000), and *in vivo* in MCF-7 xenograft breast cancer model (Foster et al., 2006), and also causes regression of estrone sulphate-stimulated nitrosomethylurea-induced mammary tumours in ovariectomized rats (Purohit et al., 2000). Moreover, Irosustat was the first STS inhibitor to be tested in phase I clinical trials for the treatment of postmenopausal women with advanced metastatic hormone-dependent breast cancer, showing encouraging results (Stanway et al., 2006; Palmieri et al., 2011). More recently, STS inhibitors have shown that, in addition to breast cancer therapy may be useful for the treatment of other steroid hormone-dependent cancers such as prostate cancer (Selcer et al., 2002).

Irosustat structure is a tricyclic coumarin-based sulphamate (shown in Fig. 1A). The presence of the sulphamoyl-ester group is indispensable for its STS inhibitory activity, and, in addition, confers to the Irosustat molecule the ability to bind and to irreversibly inhibit carbonic anhydrase II (Ho et al., 2003; Lloyd et al., 2005), an enzyme that is highly expressed in mammalian erythrocytes. Irosustat undergoes spontaneous de-sulphamoylation in aqueous solutions at nearly physiologic pH (Ireson et al., 2003), leading to the formation of its major

degradation derivative, 667-Coumarin (structure shown in Fig. 1B), a process that is enhanced by increasing temperature. The binding to carbonic anhydrase II enzyme induces Irosustat uptake and transport by red blood cells, while preventing it from degradation (Ireson et al., 2004).

During the early development phases of a new drug candidate, *in vitro* metabolism studies give essential information in order to help to select the most suitable species for toxicological studies, and to provide valuable foresight on metabolic pathways in humans. To this purpose, several *in vitro* test systems from different species and sexes, such as liver microsomes and hepatocytes, are commonly used in drug metabolism assessments. In the present work, the metabolic profile, the metabolite identification and the potential species differences in the *in vitro* metabolism of Irosustat were characterized using pooled liver microsome preparations from rats, dogs, monkeys and humans, and hepatocytes from rat, dog and humans. Moreover, the enzymes participating in the Irosustat metabolism in humans were also investigated in order to help to predict possible drug-drug interactions.

DMD Fast Forward. Published on April 4, 2011 as DOI: 10.1124/dmd.111.038315
This article has not been copyedited and formatted. The final version may differ from this version.

Methods

Chemicals. Compounds Irosustat (molecular weight of free base: 309.3, purity by HPLC 99.6%) and 667-Coumarin (molecular weight of free base: 230.3, purity by HPLC 99.1%) were synthesized in Panchim (Evry Cedex, France). ^{14}C-Irosustat (specific activity 123 mCi/mmol, radiochemical purity by HPLC 98.7%) was custom labelled in GE Healthcare (Little Chalfont, Buckinghamshire UK). All reagents including all cytochrome P450 (CYP)-specific inhibitors were purchased from Sigma-Aldrich (St. Louis, MO, USA), except where indicated otherwise. Solvents used for HPLC analysis were of analytical or HPLC grade. Male and female Sprague-Dawley rat hepatocytes and liver microsomes, liver microsomes from male Beagle dogs and from male and female Cynomolgus monkeys were prepared in house. Female human liver microsomes (HLM), female Beagle dog liver microsomes, and the Reaction Phenotyping Kit v7 (consisting of HLM from 16 separate donors) were purchased from Xenotech, LLC (Lenexa, KS, USA). Fresh male Beagle dog hepatocytes and cryopreserved female human hepatocytes were purchased from Biopredic (Rennes, France). Male HLM; commercial microsomes from Baculovirus-insect cell-expressed human CYPs (Supersomes®): 1A1, 1A2, 1B1, 2A6, 2B6, 2C8, 2C9*1, 2C19, 2D6*1, 2E1, 3A4, 3A5 and CONTROL; human UDP-glucuronosyl transferases (UGTs): 1A1, 1A3, 1A4, 1A6, 1A7, 1A8, 1A9, 1A10, 2B4, 2B7, 2B15 and 2B17; and human flavin-containing monooxygenase 3 (FMO3); were all purchased from BD-Gentest (Woburn, MA, USA). Human Sulfotransferases (SULTs): 1A1*1 and 1A3 were purchased from Cypex (Dundee, Scotland, UK), and SULTs 1A1*2 and 1A2*1 from Invitrogen (Carlsbad, CA, USA). All liver-derived samples were obtained with permission from the ethics committees from Ipsen Pharma S.A. and the other local manufacturers.

Preparation of Liver Microsomes. Liver samples were excised and washed in isotonic saline. All subsequent steps were carried out at 4ºC. The liver was placed on crushed ice, minced with scissors, and then homogenized in 50 mM Tris-HCl buffer (pH 7.4) containing 154 mM KCl, using a Potter-Elvehjem homogenizer. The homogenate was centrifuged at 10,000 x g at 4ºC for 20 min, and the resulting pellet was discarded. The supernatant was centrifuged at 100,000 x g at 4ºC for 1 h (Lake, 1987), and the pellet (microsomes) resuspended in 50 mM Tris-HCl buffer pH 7.4 containing 154 mM KCl. The protein concentration was adjusted to 20 mg/ml, and the resulting microsomal suspensions were aliquoted and stored at -80°C. Microsomes were characterized by determination of total content of cytochrome P450 (Omura and Sato, 1964), and by determination of cytochrome C (P450) reductase (Lake, 1987), ethoxycoumarin O-deethylase (Peters et al., 1991) and testosterone 6β-hydroxylase activities (Kawano et al., 1987).

Hepatocyte Isolation and Culture. Male and female Sprague-Dawley rats (180-220 g) were anesthetized with ketamine / medetomidine (10 mg / 0.1 mg). After loss of the righting reflex, an abdominal midline incision was made and the portal vein was cannulated. Hepatocytes were further isolated by a collagenase perfusion method adapted from Seglen, 1976; and Gomez-Lechon et al., 1992. After wash in a suspension medium (50% L-15 medium Leibovitz and 50% nutrient mixture F-12 HAM medium, containing 5% foetal calf serum, 0.94 mg/ml D+glucose, 2 mg/ml bovine serum albumin, 2 mM L-glutamine, 10 mM $HNaCO_3$, 100 IU-µg/ml penicillin-streptomycin, and 10^{-8} M insulin), the viability and cell density were measured by the trypan blue exclusion method using an haemocytometer. Finally, rat hepatocytes were plated in 24-well culture dishes coated with collagen substratum (cell density: 25 x 10^4 viable cells/well). Fresh male Beagle dog hepatocytes were purchased already plated in 24-well culture dishes coated with collagen substratum (cell density: 3 x 10^4 viable cells/well). Female human cryopreserved

hepatocytes were thawed according to the instructions provided by the supplier, and the viability and cell density were measured by the trypan blue exclusion method. Finally, human hepatocytes were plated in 24-well culture dishes coated with collagen substratum (cell density: 0.4 x 10^6 viable cells/well).

Incubation of ^{14}C-Irosustat with Liver Microsomes and Determination of Apparent Intrinsic Clearance. Liver microsomes (1 mg/ml) from Sprague-Dawley rats, Beagle dogs, Cynomolgus monkeys and humans (both sexes separately) were incubated in duplicate with 25 µM ^{14}C-Irosustat at 37ºC in 50 mM Tris-HCl buffer pH 7.4 containing 5 mM $MgCl_2$, and in the presence of a NADPH-generating system consisting of: 4 mM D-glucose 6-phosphate, 2 IU/ml glucose 6-phosphate dehydrogenase and 1 mM β-NADP (0.5 ml final volume). The reactions were started by addition of β-NADP, and were quenched at 0, 30, 60 and 120 min, by addition of one volume of acetonitrile containing 10% acetic acid. Incubation mixtures without microsomes and without β-NADP incubated for 120 min were used as controls. The samples generated were either stored at -80ºC until analysis or directly analysed by HPLC after centrifugation at 20,000 x g at 4°C for 15 min and further dilution with HPLC mobile phase.

For each species and sex, the apparent intrinsic clearance ($Cl_{int,app}$) parameter was estimated using the $t_{1/2}$ method, where the log-percent of substrate remaining versus time was plotted. For calculation, data from incubations up to 30 min were selected. Since 667-Coumarin is formed by degradation during the incubations, and both Irosustat and 667-Coumarin actually act as a substrate, the percent remaining included both compounds enabling the estimation of the CYP-mediated $Cl_{int,app}$. The slope of the resulting linear regression (-k) was used to obtain *in vitro* $t_{1/2}$ (*in vitro* $t_{1/2}$ = 0.693 / k). The *in vitro* $t_{1/2}$ was further converted to $Cl_{int,app}$ using the following equation: $Cl_{int,app}$ = [(0.693 / *in vitro* $t_{1/2}$) • (ml incubation / mg microsomes) • (45 mg microsomes

/ g liver) • (X g liver / kg body weight)], where X = 45 for rat, 25 for dog, 30 for monkey, and 20 for human (Bohnert and Gan, 2010).

Incubation of Unlabelled Irosustat with Hepatocytes. Cultured hepatocytes from male and female Sprague-Dawley rats, male Beagle dog and woman, were incubated in duplicate with 50 µM unlabelled Irosustat at 37ºC in a humidified atmosphere containing 95% air and 5% CO_2. The incubation volume was 0.5 ml and the incubation time period was 3 hours. The incubations were quenched by addition of one volume of acetonitrile containing 3% acetic acid. The samples generated were either stored at -80ºC until analysis or directly analysed by HPLC after centrifugation at 20,000 x g at 4°C for 15 min, and dilution with HPLC mobile phase.

Incubation of Unlabelled Irosustat and 667-Coumarin with Rat Liver Microsomes and Rat Hepatocytes. Liver microsomes (1 mg/ml) and hepatocytes from female Sprague-Dawley rats were incubated either with 50 µM Irosustat or with 50 µM 667-Coumarin for 120 minutes (liver microsomes) and 3 hours (hepatocytes), under the same conditions as previously described.

Estimation of the Apparent K_M and V_{max} for Irosustat Metabolism in HLM. Prior assessment of the enzyme kinetics, the linearity of ^{14}C-labelled Irosustat transformation in HLM was evaluated in a range of increasing microsomal protein concentrations, and incubation time periods. Linear metabolite formation was found up to approximately 1 mg microsomal protein per ml, and up to 40 minutes incubation, respectively (data not shown). These incubation conditions were selected for the enzyme kinetics experiment. The microsomal incubations were conducted with final ^{14}C-Irosustat concentrations of 0, 5, 10, 25, 50, 80, 110, 150 and 250 µM (n=4 for each concentration, except for 110 and 150 µM, which were n=2). Reactions were

quenched and samples analysed with on-line radioactivity detection as described below. Apparent K_M and V_{max} were estimated after fitting the Michaelis-Menten equation: $V = V_{max} \cdot S/(K_M+S)$ to the obtained data, using the WinNonlin version 3.3 software (Pharsight, Mountain View, CA, USA).

Determination of the Human CYP Enzymes Responsible for Irosustat Metabolism. The main CYP enzymes responsible for the formation of phase I metabolites of Irosustat were identified using three complementary approaches:

Correlation Study with CYP Isoform-Specific Activities in HLM. The Irosustat biotransformation rate (as metabolite formation) in incubations of the test compound with a panel of 16 individual batches of characterized HLM, was correlated with the rate of 13 probe CYP-specific reactions: 7-ethoxyresorufin O-dealkylation and phenacetin O-deethylation (for CYP1A2), coumarin 7-hydroxylation (for CYP2A6), S-mephenytoin N-demethylation and bupropion hydroxylation (for CYP2B6), paclitaxel 6α-hydroxylation (for CYP2C8), diclofenac 4'-hydroxylation (for CYP2C9), S-mephenytoin 4'-hydroxylation (for CYP2C19), dextromethorphan O-demethylation (for CYP2D6), chlorzoxazone 6-hydroxylation (for CYP2E1), testosterone 6β-hydroxylation and midazolam 1'-hydroxylation (for CYP3A4/5), and benzydamine N-oxidation (for FMO). The incubations (n=2) were carried out with 50 μM unlabelled Irosustat and 1 mg/ml microsomal protein concentration for 40 minutes, under the conditions previously described for incubations of Irosustat with liver microsomes. The results of activity assays using specific cytochrome P450 substrates were taken from the data sheet supplied by the microsome manufacturer (Reaction phenotyping kit, Xenotech, LLC, Lenexa, KS, USA). The *Pearson Correlation Coefficient (r)* was estimated and the correlation was

accepted as significant when the probability level was lower than 0.01 (α=0.01). NCSS 2001 software (Kaysville, UT, USA) was used for calculation.

Chemical Inhibition of CYP Enzymes in Pooled HLM. Incubations of 50 µM Irosustat in the presence and absence of 10 specific CYP inhibitors (n=2, except for the CYP2C19 inhibitors nootkatone and (+)-N-3-benzyl-nirvanol, n=3) were performed using pooled HLM under the incubation conditions described above. The following chemical inhibitors and final concentrations were used (all working solutions were made in DMSO): 1 µM furafylline (CYP1A2, mechanism-based inhibitor); 0.1 µM methoxsalen (CYP2A6, mechanism-based inhibitor); 750 µM orphenadrine (CYP2B6 reversible inhibitor); 10 µM quercetin (CYP2C8, reversible inhibitor); 2 µM sulfaphenazole (CYP2C9, reversible inhibitor); 100 µM nootkatone and 5 µM (+)-N-3-benzyl-nirvanol (CYP2C19, reversible inhibitors); 0.5 µM quinidine (CYP2D6, reversible inhibitor); 15 µM 4-methylpyrazole (CYP2E1, reversible inhibitor), and 0.5 µM ketoconazole (CYP3A4/3A5, reversible inhibitor). For the mechanism-based inhibitors furafylline and methoxsalen, HLM were pre-incubated for 15 minutes in the presence of inhibitor and NADPH-generating system before addition of Irosustat.

Incubation with cDNA-Expressed Human Enzymes. 50 µM unlabelled Irosustat was incubated (n=2) for 60 minutes with insect cell microsomes expressing individual human CYP enzymes (Supersomes®, 100 pmol CYP/ml): CYP1A1, 1A2, 1B1, 2A6, 2B6, 2C8, 2C9*1, 2C19, 2D6*1, 2E1, 3A4, 3A5. Irosustat was also incubated with 500 µg/ml FMO3, CONTROL non-enzyme expressing insect cell microsomes, and additionally with CYP2B6 at shorter incubation times (10, 20 and 40 min). The incubations were carried out at 37ºC as described previously. The metabolism of 50 µM unlabelled 667-Coumarin by the described cDNA-expressed human enzymes was also investigated following the same incubation conditions.

DMD Fast Forward. Published on April 4, 2011 as DOI: 10.1124/dmd.111.038315
This article has not been copyedited and formatted. The final version may differ from this version.

Investigation of the Role of CYP1A2 in Irosustat Metabolism. Native pooled HLM and CYP1A2-fortified HLM showing two-fold increased CYP1A2 activity were used for these experiments. In order to prepare CYP1A2-fortified HLM, phenacetin O-deethylase activity was determined in both, CYP1A2 Supersomes® and pooled HLM, using 500 µM phenacetin as substrate (concentration at V_{max}). The data resulting from this test indicated that the concentration of recombinant human CYP1A2 necessary to increase two-fold the CYP1A2 activity in the HLM suspension was 20 pmol/ml (data not shown). For the main experiment, 50 µM unlabelled Irosustat was incubated with native pooled HLM (1 mg/ml) or CYP1A2-fortified HLM (1 mg/ml plus 20 pmol/ml CYP1A2) in the presence/absence of a mix of CYP chemical inhibitors (10 µM quercetin, 2 µM sulfaphenazole, 20 µM tranylcypromine and 0.5 µM ketoconazole). In all cases, incubations were performed in the presence/absence of 1 µM furafylline. The incubations (n=2) were carried out for 40 minutes after 15 minutes preincubation with or without furafylline, under the conditions previously described.

Determination of the Phase II Enzymes Responsible for the Metabolism of Irosustat.

Human UGTs. Preliminary results indicated that cDNA-expressed human CYP1A2 is able to reproduce the metabolite profile of Irosustat obtained in HLM. Therefore, unlabelled Irosustat was incubated with CYP1A2 Supersomes® (200 pmol CYP/ml). After 120 min incubation, UGT individual human enzymes (1 mg/ml final concentration, n=2): UGT1A1, 1A3, 1A4, 1A6, 1A7, 1A8, 1A9, 1A10, 2B4, 2B7, 2B15 and 2B17 were added to the incubates together with 2 mM UDP-glucuronic acid, 0.025 mg/ml alamethicin and $MgCl_2$ supplementary solution (10 mM final concentration). The incubation volume was 400 µl, and the reactions were quenched after 120 min from UGT addition with one volume of acetonitrile containing 10% acetic acid.

Human SULTs. As in the case of human UGTs, unlabelled Irosustat was first incubated with 200 pmol/ml CYP1A2 Supersomes®. After 120 min incubation, SULT individual human enzymes (12.5 µg/ml final concentration, n=2): SULT1A1*1, SULT1A1*2, SULT1A2*1 and SULT1A3 were added to the incubates together with 50 µM adenosine 3'-phosphate 5'-phosphosulphate, 10 mM dithiothreitol and $MgCl_2$ supplementary solution (5 mM final concentration). The incubation volume was 400 µl, and the reactions were quenched after 120 min from SULT addition with one volume of acetonitrile containing 10% acetic acid.

Formation of glucuronide and sulphate conjugates of 667-Coumarin. Unlabelled 667-Coumarin was directly incubated (n=2) with the described human UGT and SULT enzymes, under the same conditions of incubation but without the pre-incubation step with CYP1A2 Supersomes® .

HPLC Analysis. ^{14}C-Irosustat and its metabolites were separated by HPLC using a Waters 600 solvent delivery system equipped with a reversed-phase column Sunfire C_{18}, 150 x 4.6 mm, 5 µm particle size from Waters (Milford, MA, USA). The mobile phase consisted of 50 mM ammonium formiate pH 5.0 (solvent A) and methanol (solvent B), and the flow rate was 1 ml/min. The initial mobile phase contained 25% solvent B and was maintained at this composition for 2 min. The percentage of solvent B was increased linearly up to 53% over the next 24 min, and further increased to 70% in the following 7 min. The percentage of solvent B was rapidly changed to 100% in 0.1 min, and maintained at this composition for 5 min. Finally, the percentage of solvent B was returned to 25% in the last 7 min. On-line radiochemical detection was performed using a LB508 radioflow detector equipped with 150 µl-solid scintillation cell (YG-150) from Berthold Technologies (Bad Wildbad, Germany). When using non-radiolabeled Irosustat, UV peak detection was made using a Waters 486 variable wavelength

or a Waters 2487 dual λ absorbance detector (Milford, MA, USA) at 312 nm. Occasionally, the HPLC column was replaced by a Symmetry C_{18}, 250 x 4.6 mm, 5 µm particle size or a Sunfire C_{18}, 100 x 4.6 mm, 3.5 µm particle size (both from Waters), the gradient times and the flow rate were adjusted to the column dimensions when necessary.

Mass Spectrometric Characterization. Metabolites in representative incubate samples were selected for LC-MS characterization. Monitoring of metabolite ions was conducted using a ZQ2000 mass spectrometer (Waters, Milford, MA, USA) over the regions where HPLC peaks were present. The mass spectrometer operated with an electrospray ion source in positive ionization mode. Data were captured by means of full scan mass spectra. The capillary and extractor voltages were set at 3 kV and 3 V, respectively; the RF lens voltage was set at 0.5 V; the source and desolvation temperatures were set at 120ºC and 250°C, respectively; and the desolvation and cone gas flow rates were 400 and 50 L/h, respectively. Two cone voltages (30V and 60V) were used in order to determine the fragmentation pattern of the compounds. The spectra obtained in chromatograms from incubates with Irosustat or 667-Coumarin were compared to blank samples. Data was acquired by Masslynx 4.0 software (Waters, Mildford, MA, USA).

Phase I Metabolite Isolation. The main phase I metabolites were produced by incubating 50 µM Irosustat or 667-Coumarin with rat liver microsomes (2 mg/ml protein concentration) over 120 minutes as previously described. Incubates were centrifuged and the supernatants diluted with 50 mM ammonium formiate pH 5.0. The metabolites were purified by solid phase extraction (SPE) using SEP-PAK PLUS C-18 cartridges (Waters, Milford, MA, USA). SPE cartridges were activated with acetonitrile and further conditioned with 50 mM ammonium formiate pH 5.0. Then, diluted supernatants (5 ml) were loaded onto each SPE cartridge, and a washing step was

carried out with 50 mM ammonium formiate pH 5.0. Metabolites were eluted using 2 ml acetonitrile. The SPE fractions were pooled and dried under stream of nitrogen and the dry residues were reconstituted into 50 mM ammonium formiate pH 5.0 containing 17% acetonitrile. Metabolites were separated by HPLC with a Symmetry C_{18} column (250 x 4.6 mm, 5 µm, Waters, Milford, MA, USA), and purifed by fraction collection of HPLC elutes. The isolated metabolite fractions were freeze-dried on a Christ Alpha 2-4 Lyophilizer (B.Braun-Biotech, Melsungen, Germany). Freeze-drying procedure was repeated three times.

NMR Analysis of Isolated Metabolites Lacking Sulphamoyl Group. The characterisation of the chemical structure of isolated 667-Coumarin derivatives was performed by NMR (*Serveis Cientifico-técnics*, University of Barcelona, Spain). NMR experiments were carried out on either a 600- or 800-MHz Avance NMR spectrometer fitted with TCI H-C/N-D-05 cryoprobes (Bruker, Wissembourg Cédex, France). Samples of the isolated metabolites were dissolved in dimethylsulfoxide-d6, and NMR data sets were acquired at 25°C. The experiments carried out were: monodimensional ^{1}H-NMR spectra; two dimensional homonuclear ^{1}H-^{1}H correlation experiments (correlation spectroscopy and total correlation spectroscopy); and two dimensional heteronuclear ^{1}H-^{13}C correlation experiments (heteronuclear single quantum correlation and heteronuclear multiple bond correlation).

Identification of Irosustat Primary Metabolites (containing sulphamoyl group). Isolated Irosustat primary metabolites were incubated in aqueous buffer at pH 7-8 at 37ºC for 2.5 h in order to induce de-sulphamoylation. The resulting 667-Coumarin derivatives where compared to the NMR identified ones by HPLC co-elution experiments.

DMD Fast Forward. Published on April 4, 2011 as DOI: 10.1124/dmd.111.038315
This article has not been copyedited and formatted. The final version may differ from this version.

β-Glucuronidase Treatment. Some of the main phase II metabolites of Irosustat were tentatively identified by LC-MS as glucuronides of a number of oxidized derivatives of 667-Coumarin. To assess the identity of the aglycones (actually phase I metabolites), the glucuronides were obtained by incubation of Irosustat with hepatocytes, and purified by fraction collection of HPLC elutes. The fractions containing each metabolite were pooled and dried under stream of nitrogen. After dilution with 50 mM ammonium formiate pH 5.0 the specimens were freeze-dried. The conjugated metabolites were individually incubated with 3.75 mg/ml β-glucuronidase enzyme (from *Helix pomatia*, Type H-1, Sigma-Aldrich, St. Louis, MO, USA) in 100 mM sodium acetate buffer pH 5.0, at 37ºC for 6 h. The incubations were quenched by addition of acetonitrile containing 10% acetic acid. All the samples generated were analysed by HPLC and the resulting phase I metabolites where compared to the already identified ones by HPLC co-elution experiments.

DMD Fast Forward. Published on April 4, 2011 as DOI: 10.1124/dmd.111.038315
This article has not been copyedited and formatted. The final version may differ from this version.

Results

***In Vitro* Metabolite Profile of ^{14}C-Irosustat in Liver Microsomes from Different Species and Sexes.** The *in vitro* metabolic profile of ^{14}C-Irosustat in liver microsomes was compared among rats, dogs, monkeys and humans (males and females separately). The relative percentage of peak area in the radio-HPLC profiles for each metabolite after 120 minute incubations is presented in Table 1. Considering all species/sexes during the whole time-course experiments, up to 15 different labelled metabolites of ^{14}C-Irosustat were detected. The obtained radio-HPLC metabolite profiles were analogous to those obtained by UV detection at 312 nm. A representative HPLC-UV profile of a HLM incubate is shown in Fig. 2A.

The ^{14}C-Irosustat metabolites showing a percentage of radioactive peak area higher than 5% were considered as main metabolites. In liver microsomes from the different species under study, the main metabolites were: M7, M8, M13, M14, M16 and 667-Coumarin. They were found in all samples, except for M14 which was not detected in female monkey microsome incubates, appearing only in males. Besides these main metabolites, some minor metabolites accounting for relative percentages below 4.4%, were also detected and showed some differences among species and/or between sexes, although these differences were not considered as relevant.

Taking into account $Cl_{int,app}$ parameters (Table 2), the highest transformation rate of ^{14}C-Irosustat was observed in monkey liver microsomes (faster in females than in males), followed by rat, dog and human microsomes. The fastest metabolism rate in monkeys was associated with increased production of metabolites M7 and M8 as compared with the other species (see Table 1).

The *in vitro* metabolite profile of ^{14}C-Irosustat in dog liver microsomes was the closest to the one obtained in HLM both qualitatively and quantitatively, except for metabolite M11 that was detected in human but not in dog microsomes.

Results from control samples without microsomes demonstrated that Irosustat is hydrolyzed to 667-Coumarin under the incubation conditions (at 37ºC and pH 7.4). However, the amount of 667-Coumarin formed in these samples was lower than the amount formed in control samples containing microsomes without ß-NADP (Table 2).

***In Vitro* Metabolite Profile of Irosustat in Hepatocytes from Different Species.** As shown in Fig. 2, the pattern of Irosustat metabolism by hepatocytes was remarkably different from the one obtained with liver microsomes. Five main metabolites of Irosustat were detected in incubations with human hepatocytes: M1, M2, M12, M17 and 667-Coumarin (Fig. 2B). Except for 667-Coumarin, these metabolites were not formed in the microsome incubations, suggesting that most of them might be phase II metabolites. Fig. 2C and 2D also shows the metabolite profile of Irosustat in hepatocytes from rat and dog, respectively: six main peaks in addition to 667-Coumarin (M2, M3, M7, M12 and M17) were detected in rat hepatocytes, and in dog, the main metabolites detected were M12, M17 and 667-Coumarin.

Determination of the Human CYP Enzymes Responsible for the Metabolism of Irosustat. As a previous step to the enzyme identification experiments, the substrate concentration-dependent transformation of ^{14}C-Irosustat was assessed in HLM. The kinetics showed a classical hyperbolic pattern (data not shown), and therefore, the Michaelis-Menten kinetics equation was fitted to the metabolite formation data giving a K_M value of 43.4 µM and a V_{max} value of 369 pmol/ml/min. From these results and former data on linearity of ^{14}C-Irosustat

DMD Fast Forward. Published on April 4, 2011 as DOI: 10.1124/dmd.111.038315
This article has not been copyedited and formatted. The final version may differ from this version.

metabolism, the incubation conditions selected for the following phenotyping experiments were set as follows: 50 µM Irosustat, 1 mg/ml microsomal protein concentration and 40 min incubation time.

In order to identify the CYP enzymes responsible for the metabolism of Irosustat, a combination of three experimental approaches was performed: (a) correlation analysis of Irosustat phase I metabolite formation rate with several CYP isoform-specific activities in a panel of 16 individual HLM; (b) assessment of the effect of chemical CYP isoform-specific inhibitors on Irosustat metabolite formation in pooled HLM; and (c) formation of Irosustat metabolites by cDNA-expressed CYP enzymes. Variable results were obtained for each approach. The correlation between specific CYP activities and Irosustat metabolite formation appeared as probably the most selective part of the study and the results are shown in Table 3. Under our experimental conditions, the formation of all Irosustat metabolites, except for P-36, correlated with the activity of one or more of the members of CYP2C family (i.e. CYP2C8, CYP2C9 and CYP2C19). For some of the metabolites, additional correlation was found with CYP3A4/5 (M13, M14 and M16), and CYP2E1 (M7) activities. Metabolite P-36 did not correlate with any of the CYPs tested. The results of the chemical inhibition phase (Table 4) showed that almost all used inhibitors, except those for CYP1A2 (furafylline) and CYP2C19 (nootkatone and (+)-N-3-benzyl-nirvanol), relevantly decreased the formation of several Irosustat metabolites. Table 5 shows the results obtained in incubations of cDNA-expressed CYP enzymes with Irosustat. Recombinant CYP1A2 and CYP2C19 were able to form most of the Irosustat metabolites produced in HLM incubations. CYP2A6 and FMO enzymes were not able to metabolize Irosustat. Since CYP2B6 was able to form M16 and P-36 but not its respective sulphamoylated precursors M13 and M18, CYP2B6 was additionally incubated with Irosustat for shorter

incubation times showing the formation of M18 but not M13. 667-Coumarin was also incubated with the same cDNA-expressed CYP enzymes. The 667-Coumarin metabolites: M8, M16 and P-36, were formed by different enzymes. M8 was formed by the same enzymes as Irosustat; M16 was formed by the same enzymes as Irosustat plus CYP2A6, CYP2C8 and CYP2E1; and P-36 was formed by all CYPs except for CYP2C8, CYP2C9 and CYP2E1.

Although all three approaches have advantages and disadvantages, a combination of them was required to identify which enzyme or enzymes could be potentially responsible for Irosustat metabolism. The enzymes that showed positive results in the three approaches were: CYP2C8, CYP2C9, CYP2E1 and CYP3A4/5, and were identified as the main enzymes responsible for the phase I metabolism of Irosustat.

Investigation of the Role of CYP1A2 in Irosustat Metabolism. The effect of a combination of chemical inhibitors of the CYPs involved in Irosustat metabolism was assessed in native and CYP1A2-fortified HLM, in the presence/absence of furafylline (CYP1A2 inhibitor). Table 6 shows the percentage of inhibition for each of the Irosustat metabolites formed. Furafylline alone showed no inhibitory effect either in native or in CYP1A2-fortified HLM, except for a slight inhibition of M14 formation in the latter. The formation of all metabolites was remarkably inhibited by the combination of specific CYP inhibitors in both HLM models. Approximately the same inhibition percentages were found in Irosustat incubations with native HLM when the mix of inhibitors was used either in presence or in absence of furafylline. However, in CYP1A2-fortified HLM the inhibition of Irosustat metabolism increased (for almost all metabolites) when furafylline was used together with the mix of CYP-inhibitors.

DMD Fast Forward. Published on April 4, 2011 as DOI: 10.1124/dmd.111.038315
This article has not been copyedited and formatted. The final version may differ from this version.

Determination of the Phase II Enzymes Responsible for the Metabolism of Irosustat.

To identify the relative contribution of specific human liver enzymes responsible for the formation of the phase II metabolites of Irosustat, incubations were performed using cDNA-expressed human UGT and SULT enzymes in the presence of the respective cofactors. The experimental approach consisted in incubating Irosustat with recombinant CYP1A2 in order to induce the formation of most of the phase I *in vitro* metabolites (see Table 5), followed by the addition of the different UGT and SULT enzymes and the required cofactors.

As shown in Table 7, up to nine peaks corresponding to putative glucuronides were produced by the different UGTs. These metabolites were M12 and M2 (already detected in hepatocyte incubations (Fig. 2)), and the newly detected ones: G1, G2, G3, G4, M4, G7 and G8. M12 was also formed when 667-Coumarin was incubated directly with all UGTs except for UGT1A4, which, in turn, was the unique UDP-glucuronosyl transferase unable to form any of the glucuronides.

As shown in Table 8, up to eight peaks corresponding to potential sulphate conjugates were found after incubation of Irosustat phase I metabolites with different human SULTs (1A1*1, 1A1*2, 1A2*1 and 1A3), using the same experimental approach. The sulphate conjugates were named S2, S3, S4, S5, S6 and S7 (new peaks), and were formed in addition to M17 and M3 which had already been detected in hepatocyte incubations (Fig. 2). M17 formation was also confirmed when 667-Coumarin was incubated directly with all the SULTs. Sulfotransferases SULT1A1*1, 1A1*2 and 1A2*1, but not SULT1A3, were capable to form M17. SULT1A1*1 was able to produce all the sulphate conjugates identified and also in the largest amounts.

DMD Fast Forward. Published on April 4, 2011 as DOI: 10.1124/dmd.111.038315
This article has not been copyedited and formatted. The final version may differ from this version.

Preliminary Identification of Irosustat Main Metabolites by Mass Spectrometry. The MS spectra of Irosustat and its main *in vitro* metabolites are shown in Supplemental Data 1.

The MS spectrum of Irosustat was characterized by its protonated molecular ion of *m/z* 310 and by the formation of a main fragmentation product of *m/z* 231. This fragmentation product was consistent with the protonated molecular ion of 667-Coumarin molecule, which was produced after loss of the 3-O-sulphamoyl group in the MS ion source. In addition to 667-Coumarin, the main *in vitro* Irosustat metabolites were identified as mono-oxidized derivatives, and also glucuronide and sulphate conjugates.

Mono-oxidized metabolites: Two groups of mono-oxidized metabolites were found in incubations of Irosustat with microsomes: mono-oxidized Irosustat derivatives (primary metabolites): M7, M9, M13 and M14; and mono-oxidized 667-Coumarin derivatives (secondary metabolites): M8, M15 and M16.

Differences in the fragmentation pattern of the metabolites at 60 V cone voltage (see Supplemental Data 1) and, importantly, differences in their HPLC retention time (see Fig. 2A), indicated that they are probably formed by oxidation in different atoms of the Irosustat or 667-Coumarin structure.

Glucuronide metabolites: Three glucuronide metabolites could be identified by MS in hepatocyte incubations with Irosustat: one corresponding to the 667-Coumarin glucuronide: M12; and two mono-oxidized 667-Coumarin glucuronides: M1 and M2.

Sulphate metabolites: One sulphate metabolite found in hepatocyte incubates was identified by MS as 667-Coumarin sulphate, and was named as M17.

DMD Fast Forward. Published on April 4, 2011 as DOI: 10.1124/dmd.111.038315
This article has not been copyedited and formatted. The final version may differ from this version.

***In Vitro* Incubations of 667-Coumarin with Liver Microsomes and Hepatocytes.** In order to help to the identification of Irosustat metabolites, 667-Coumarin and Irosustat were incubated separately with both female rat liver microsomes and female rat hepatocytes at 37ºC for 120 minutes and 3 hours, respectively. The metabolite profiles obtained from 667-Coumarin incubations were compared with those obtained with Irosustat. As shown in Fig. 3, M8, M11, M15, M16, M12, M17 and P-36 were formed directly from 667-Coumarin; conversely, the primary metabolites M7, M9, M13 and M14 were only formed when Irosustat was used as substrate. These results supported the metabolite identification performed by mass spectrometry.

Structure Elucidation of Irosustat Main Metabolites. The main phase I metabolites of Irosustat were purified as described in the Material and Methods section. Those compounds, corresponding to putative mono-oxidized metabolites of Irosustat, were converted to their respective 667-Coumarin counterparts by incubation at neutral pH and 37ºC temperature in order to force the de-sulphamoylation. The resulting oxidized 667-Coumarin derivatives where further characterised by its HPLC retention time. The results showed that the Irosustat oxidized metabolites or primary metabolites M7, M13, M14 and M18 were the sulphamate-containing precursors of the oxidized 667-Coumarin derivatives M8, M16, M15 and P-36 (secondary metabolites), respectively.

The identification of the chemical structure of the mono-oxidized 667-Coumarin derivatives (indeed, the position of the oxidized atoms) was performed by NMR, and the identification of their respective sulphamate-containing derivatives was automatically deduced from the previously described data (see Fig. 4). In the case of M8 and M16, their monodimensional ^{1}H spectra indicated that no changes took place in the aromatic region with respect to 667-Coumarin. The same conclusion was achieved for M15 after interpretation of the

DMD Fast Forward. Published on April 4, 2011 as DOI: 10.1124/dmd.111.038315
This article has not been copyedited and formatted. The final version may differ from this version.

homonuclear ^{1}H-^{1}H correlation spectroscopy and total correlation spectroscopy and heteronuclear ^{1}H-^{13}C single quantum correlation and multiple bond correlation two-dimension spectra. For all three cases, these spectra indicated that the hydroxyl group was located in the cycloheptane ring. The position of the hydroxyl group in the cycloheptane ring was determined from the study of the ring atoms in two-dimensional spectra. Thus, metabolites M8, M15 and M16 were hydroxilated at the C10, C12 and C8 positions in the cycloheptane ring of 667-Coumarin molecule, respectively. Obviously, the same hydroxylation sites corresponded to their sulphamate-containing counterparts M7, M14 and M13. The structures described in Fig. 4 for these metabolites are compatible with the NMR data.

The glucuronidation and the sulphation of 667-Coumarin may basically be formed through its unique hydroxyl group at C3 position, yielding M12 (667-Coumarin 3-O-glucuronide) and M17 (667-Coumarin 3-O-sulphate), respectively (see Fig. 4). Metabolites M1 and M2, which were preliminary identified by mass spectrometry as glucuronides (Table 9), were purified and treated with β-glucuronidase, leading to the formation of M11 and M16, respectively (see Fig. 4).

DMD Fast Forward. Published on April 4, 2011 as DOI: 10.1124/dmd.111.038315
This article has not been copyedited and formatted. The final version may differ from this version.

Discussion

The novel STS inhibitor Irosustat was extensively metabolized *in vitro* in liver microsomes and hepatocytes. Its metabolite profile was similar among the species tested and between sexes. However, marked differences were found between both *in vitro* systems, meaning that phase I and phase II enzymes are involved in Irosustat metabolism. Various mono-oxidized metabolites of Irosustat (primary metabolites) and of its de-sulphamoylated derivative 667-Coumarin (secondary metabolites) were formed in liver microsomes; therefore, oxidation was the predominant route of Irosustat phase I metabolism. The most abundant mono-oxidized metabolites were identified by NMR showing hydroxyl groups at different carbon atoms of the cycloheptane ring. As shown in Table 1 and Fig. 4, the main primary phase I metabolites were: M7, M13 and M14 (10-hydroxy-, 8-hydroxy- and 12-hydroxy-Irosustat, respectively); and the corresponding secondary phase I metabolites were: M8, M16 and M15 (10-hydroxy-, 8-hydroxy- and 12-hydroxy-667-Coumarin, respectively). On the other hand, the main metabolites in hepatocyte incubations were formed by phase II metabolic enzymes. This fact was further demonstrated by LC-MS analysis. Rat, dog and human hepatocytes mainly converted Irosustat to 667-Coumarin and to 3-O-glucuronide and 3-O-sulphate conjugates of 667-Coumarin (M12 and M17, respectively). In human hepatocytes, M1 and M2 derivatives were also formed and were identified as glucuronides of metabolites M11 and M16 (both 667-Coumarin derivatives), respectively. However, the chemical structures of M1 and M2 were not fully determined. Since hepatocytes are a more physiologically significant *in vitro* model, a high relevance of phase II metabolism is anticipated *in vivo*.

DMD Fast Forward. Published on April 4, 2011 as DOI: 10.1124/dmd.111.038315
This article has not been copyedited and formatted. The final version may differ from this version.

The comparison of the microsomal metabolites of Irosustat allowed us to detect metabolic similarities between animal species and humans. These results should be helpful when selecting the non-rodent species for toxicity evaluation. Qualitatively, all phase I human metabolites were formed by dog microsomes except for metabolite M11. Nevertheless, M11 was formed in rats, indicating that no unique human metabolites were formed in liver microsomes, and therefore no safety concerns are anticipated from the *in vitro* data. Quantitatively, the following rank order was established among species regarding Irosustat $Cl_{int,app}$ (see Table 2): monkey>>rat >dog≥humans. As a conclusion, the dog was the species that showed the closest metabolic pattern to humans.

Under *in vitro* incubation conditions (at 37ºC and pH 7.4), 667-Coumarin was the major degradation product of Irosustat formed by hydrolysis of the sulphamoyl-ester group (Fig. 1). De-sulphamoylation in aqueous solution probably occurs *via* E1cB elimination reaction, assisted by the extended conjugation present in the coumarin motif (Lloyd et al., 2005). However, the results of the present work showed how incubations of Irosustat with microsomes in the absence of cofactor produced increased amounts of 667-Coumarin as compared to incubations of Irosustat in buffer alone (Table 2), demonstrating that 667-Coumarin can be also formed by non-NADPH-dependent enzymatic hydrolysis. Therefore, 667-Coumarin may be considered as a metabolite and not only a degradation product. Moreover, 667-Coumarin was previously described to be a product resulting after STS inhibition by Irosustat (Woo et al., 2000). Since the STS enzyme is present in liver microsomes (Kauffman et al, 1998), STS is a probable candidate for the enzymatic formation of 667-Coumarin.

Once the main metabolites of Irosustat were identified and considering the various phase I and phase II reactions involved, a careful evaluation of the enzymes capable of metabolising

DMD Fast Forward. Published on April 4, 2011 as DOI: 10.1124/dmd.111.038315
This article has not been copyedited and formatted. The final version may differ from this version.

Irosustat was assessed. Fig. 4 summarizes the *in vitro* metabolism pathways of Irosustat including the enzymes considered as responsible for its primary metabolism (those showing positive results in the correlation, inhibition and recombinant enzyme approaches): M7 was formed by CYP2C9 and CYP2E1; M9 by CYP2C8; M13 by CYP2C8, CYP2C9, and CYP3A4/5; M14 by CYP3A4/5; and M18 by CYP2C9. Although the secondary metabolites M8, M11, M15, M16 and P-36 were included in the phenotyping experiments, the identification of the enzymes involved in their formation should be considered as not fully elucidated. This is because de-sulphamoylated derivatives can be formed by two sequential reactions: (a) Irosustat hydroxylation and further hydrolysis of the sulphamoyl group; or (b) loss of the sulphamoyl group followed by hydroxylation. These two ways were demonstrated in the present work, first, by converting hydroxylated Irosustat metabolites into their respective 667-Coumarin counterparts by incubation at neutral pH and at 37ºC; and second, by direct incubation of 667-Coumarin with rat microsomes and hepatocytes (Fig. 3), and with recombinant human CYPs. Due to the structural similarities between Irosustat and 667-Coumarin, it is likely that the same enzymes could be involved in the transformation of both compounds. From the correlation and chemical inhibition tests (Tables 3 and 4), no relevant differences in phenotyping between the primary metabolites and the respective secondary ones were obtained, except for CYP2E1 which is related to M7 formation but not to M8. In the recombinant CYPs approach, Irosustat and 667-Coumarin were transformed by almost the same enzymes. However, some main differences were obtained: (a) CYP2A6 was able to metabolize 667-Coumarin but not Irosustat; (b) CYP2C9 was able to metabolize Irosustat but not 667-Coumarin; and (c) CYP2B6 formed M16 from 667-Coumarin but was not able to form M13 from Irosustat. These different capabilities of CYP2A6, CYP2B6, and CYP2C9 to metabolize Irosustat and 667-Coumarin were considered as not relevant given the high number of enzymes involved in the metabolism of both compounds.

Surprising results were obtained for CYP1A2 and CYP2C19 enzymes when the recombinant CYPs approach was assessed. The incubation of Irosustat with CYP1A2 Supersomes® showed that this enzyme was able to produce a metabolite profile very similar to the one obtained by pooled HLM. However, the two specific CYP1A2 activities measured in the 16 individual HLM batches, 7-ethoxyresorufin O-dealkylation and phenacetin O-deethylation, did not correlate with the formation of any of the Irosustat metabolites. In addition, the CYP1A2 mechanism-based inhibitor furafylline (1 μM) had no effect on the metabolism of Irosustat in pooled HLM. The inhibition was also assessed using 10-fold increased furafylline and 10-fold reduced Irosustat concentration with similar results (data not shown). Furthermore, the inhibition extent of furafylline on Irosustat metabolism was studied comparatively in incubations with native HLM and CYP1A2-fortified HLM (Table 6). As expected, Irosustat metabolism was markedly decreased in both HLM models in the presence of a combination of CYP-specific inhibitors, confirming that Irosustat is metabolised by diverse CYP isoforms. By contrast, furafylline (either alone or in combination with the mix of CYP-inhibitors) showed negligible effect in native HLM, while in CYP1A2-fortified HLM it essentially enhanced the inhibition induced by the other CYP-inhibitors, meaning that several CYPs must be affected at the same time in order to produce any potential metabolic interaction outcome.

Concerning CYP2C19, the S-mephenytoin 4'-hydroxylation activity in 15 individual HLM batches (one was considered as outlier) correlated with the formation of some of the Irosustat metabolites in HLM. In addition, the incubation of Irosustat with recombinant CYP2C19 also produced several Irosustat metabolites. However, the two specific CYP2C19 inhibitors used, nootkatone and (+)-N-3-benzyl-nirvanol (Tassaneeyakul et al, 2000; Suzuki et al, 2002), did not inhibit the formation of any Irosustat metabolite in the pooled HLM model.

DMD Fast Forward. Published on April 4, 2011 as DOI: 10.1124/dmd.111.038315
This article has not been copyedited and formatted. The final version may differ from this version.

Overall, CYP1A2 and CYP2C19 enzymes were considered as not relevant in Irosustat metabolism when other CYP enzymes are present and active. Although a minor role cannot be completely discarded (i.e. a weak contribution of CYP1A2 in case of overexpression/induction). From the phenotyping results, we may conclude that, even if co-administered drugs inhibit one of the identified drug-metabolizing enzymes, the pharmacokinetics of Irosustat is unlikely to be noticeably affected due to probable metabolic compensatory mechanisms produced by other CYP isoforms.

When Irosustat phase I metabolites were incubated with different cDNA-expressed UGTs and SULTs, up to nine different glucuronides and eight sulphates were produced, respectively. Although the actual role of each phase II enzyme was not fully clarified, phase II metabolism is a secondary pathway in Irosustat metabolism and can only occur after phase I transformation of the parent compound, or after formation of 667-Coumarin or any of its hydroxylated metabolites. Consequently, although highly involved in the overall drug disposition process, phase II enzymes would neither influence Irosustat clearance nor be the target enzymes involved in possible drug-drug interaction processes, unless the biological activity of any of the phase I metabolites was demonstrated.

To summarize, multiple Irosustat metabolic pathways including de-sulphamoylation, primary and secondary metabolism, and phase I and phase II reactions, were involved in the metabolism of Irosustat in liver microsomes and hepatocytes from several species. CYP2C8, CYP2C9, CYP3A4/5 and CYP2E1 were identified as the main enzymes responsible for the primary transformation of Irosustat. Although a number of recombinant phase II enzymes were tested with positive results, their actual clinical relevance could not be clarified. Glucuronide and sulphate conjugation reactions would be secondary to phase I transformation of Irosustat, or 667-

Coumarin formation, and therefore they should not play an important role in Irosustat clearance. The *in vitro* studies presented in this work have been also useful to identify potential metabolites of Irosustat, and to obtain valuable information for planning and interpreting future toxicology and *in vivo* metabolism of Irosustat.

DMD Fast Forward. Published on April 4, 2011 as DOI: 10.1124/dmd.111.038315
This article has not been copyedited and formatted. The final version may differ from this version.

Acknowledgements: The authors would like to thank M. Victor and C. Maté for their technical assistance, to T. Ali for his expert review, and the *Serveis Cientifico-técnics*, University of Barcelona, for performing the NMR analysis.

DMD Fast Forward. Published on April 4, 2011 as DOI: 10.1124/dmd.111.038315
This article has not been copyedited and formatted. The final version may differ from this version.

Authorship Contributions

Participated in research design: Ventura, and Solà

Conducted experiments: Ventura, and Solà

Contributed new reagents or analytic tools: Ventura, Solà

Performed data analysis: Ventura

Wrote or contributed to the writing of the manuscript: Ventura, Solà, Peraire, and Obach

Other: Celma contributed to the NMR analysis interpretation.

DMD Fast Forward. Published on April 4, 2011 as DOI: 10.1124/dmd.111.038315
This article has not been copyedited and formatted. The final version may differ from this version.

References

Bohnert T and Gan LS (2010) The role of drug metabolism in drug discovery, in *Enzyme Inhibition in Drug Discovery and Development: The Good and the Bad* (Lu C and Li AP eds) pp 91-176, Wiley, New Jersey.

Foster PA, Newman SP, Chander SK, Stengel C, Jhalli R, Woo LWL, Potter BVL, Reed MJ, and Purohit A (2006) *In vivo* efficacy of STX213, a second-generation steroid sulfatase inhibitor, for hormone-dependent breast cancer therapy. *Clin Cancer Res* **12:**5543–5549.

Foster PA (2008) Steroid metabolism in breast cancer. *Minerva Endocrinol* **33:**27-37.

Gomez-Lechon MJ, Donato MT, Ponsoda X, Jover R, and Castell JV (1992) Experimental *in vitro* models to evaluate hepatotoxicity, in *In Vitro Alternatives to Animal Pharmaco-toxicology* (Castell JV and Gomez-Lechon MJ eds) pp 92-107, Farmaindustria, Madrid.

Ho YT, Purohit A, Vicker N, Newman SP, Robinson JJ, Leese MP, Ganeshapillai D, Woo LWL, Potter BVL, and Reed MJ (2003) Inhibition of carbonic anhydrase II by steroidal and non-steroidal sulphamates. *Biochem Biophys Res Commun* **305:**909 –914.

Ireson CR, Parish D, Purohit A, Woo LWL, Potter BVL, Chander SK, and Reed MJ (2003) Development of a sensitive high performance liquid chromatography method for the detection of 667-Coumate *in vivo*. *J Steroid Biochem Mol Biol* **84(2-3):**337-342.

Ireson CR, Chander SK, Purohit A, Parish DC, Woo LWL, Potter BVL, and Reed MJ (2004) Pharmacokinetics of the Nonsteroidal Steroid Sulphatase Inhibitor 667 COUMATE and its sequestration into Red Blood Cells in Rats. *Br J Cancer* **91(7):**1399-404.

Kawano S, Kamataki T, Yasumori T, Yamazoe Y, and Kato R (1987) Purification of human liver cytochrome P-450 catalyzing testosterone 6 beta-hydroxylation. *J Biochem* **102(3):**493-501.

Kauffman FC, Sharp S, Allan BB, Burchell A, and Coughtrie MWH (1998) Microsomal steroid sulfatase: interactions with cytosolic steroid sulfotransferases. *Chem Biol Interact* **109(1-3):**169-182.

Lake BG (1987) Preparations and Characterization of Microsomal Fractions for Studies on Xenobiotics Metabolism, in *Biochemical toxicology: a practical approach* (Snell K and Mullock B eds) pp 183-215, IRL Press, Oxford, Washington DC.

Lloyd MD, Pederick RL, Natesh R, Woo LWL, Purohit A, Reed MJ, Acharya KR, and Potter BVL (2005) Crystal structure of human carbonic anhydrase II at 1.95 Å resolution in complex with 667-coumate, a novel anti-cancer agent. *Biochem J* **385:**715-720.

Omura T and Sato R (1964) The carbon monoxide-binding pigment of liver microsomes. I.-Evidence for its hemoprotein nature. *J Biol Chem* **239(7):**2370-2385.

Palmieri C, Januszewski A, Stanway S, and Coombes RC (2011) Irosustat: a first-generation steroid sulfatase inhibitor in breast cancer. *Expert Rev Anticancer Ther* **11(2)**:179-183.

Peters MM, Walters DG, van Ommen B, van Bladeren PJ, and Lake BG (1991) Effect of inducers of cytochrome P-450 on the metabolism of [3-^{14}C]coumarin by rat hepatic microsomes. *Xenobiotica* **21(4):**499-514.

Purohit A, Woo LWL, Potter BVL, and Reed MJ (2000) *In vivo* inhibition of estrone sulfatase activity and growth of nitrosomethylurea-induced mammary tumors by 667 COUMATE. *Cancer Res* **60:**3394–3396.

Reed MJ, Purohit A, Woo LWL, Newman SP, and Potter BVL (2005) Steroid sulfatase: molecular biology, regulation, and inhibition. *Endocr Rev* **26:**171–202.

Seglen PO (1976) Preparation of isolated rat liver cells. *Methods Cell Biol* **13:**29-83.

Selcer KW, Kabler H, Sarap J, Xiao Z, and Li PK (2002) Inhibition of steryl sulfatase activity in LNCaP human prostate cancer cells. *Steroids* **67(10):**821-6.

Stanway SJ, Purohit A, Woo LWL, Sufi S, Vigushin D, Ward R, Wilson RH, Stanczyk FZ, Dobbs N, Kulinskaya E, Elliott M, Potter BVL, Reed MJ, and Coombes RC (2006) Phase I study of STX 64 (667 Coumate) in breast cancer patients: the first study of a steroid sulfatase inhibitor. *Clin Cancer Res* **12:**1585–1592.

Suzuki H, Kneller MB, Haining RL, Trager WF, and Rettie AE (2002) (+)-N-3-benzyl-nirvanol and (-)-N-3-benzyl-phenobarbital: new potent and selective *in vitro* inhibitors of CYP2C19. *Drug Metab Dispos* **30(3):**235-239.

Tassaneeyakul W, Guo LQ, Fakuda K, Ohta T, and Yamazoe Y (2000) Inhibition Selectivity of Grapefruit juice components on human cytochromes P450. *Arch Biochem Biophys* **378(2):**356-363.

Woo LWL, Purohit A, Malini B, Reed MJ, and Potter BVL (2000) Potent active site-directed inhibition of steroid sulphatase by tricyclic coumarin-based sulphamates. *Chem Biol* **7:**773–791.

Footnotes

This work was sponsored by Ipsen Group.

Part of this data was previously presented in the 9th European ISSX meeting (poster abstract): Ventura V., Solà J., Peraire C. and Obach R. (2006) Metabolism of STX-64, a novel anti-cancer agent, in the rat: from *in vitro* models to *in vivo* metabolite profile, in *Drug Metab Rev* 38(1):133.

Reprint requests to be addressed to: Josep Solà

Ipsen Pharma S.A.

Crta. Laureà Miró, 395

08980 Sant Feliu del Llobregat, Barcelona (Spain)

Email: josep.sola@ipsen.com

DMD Fast Forward. Published on April 4, 2011 as DOI: 10.1124/dmd.111.038315
This article has not been copyedited and formatted. The final version may differ from this version.

Legends for Figures

Fig. 1. Chemical structures of Irosustat (A) and 667-Coumarin (B).

Fig. 2. Comparative *in vitro* HPLC-UV profiles of Irosustat metabolism in pooled human liver microsomes incubated with Irosustat for 40 minutes (A); and in hepatocytes from female human (B), male rat (C), and male dog (D) incubated with Irosustat for 3 hours. Peaks not shaded correspond to endogenous compounds present also in blank samples.

Fig. 3. Representative metabolite profiles after incubation of female rat liver microsomes with Irosustat (A) and 667-Coumarin (B) for 120 minutes; and female rat hepatocytes incubated with Irosustat (C) and 667-Coumarin (D) for 3 hours.

Fig. 4. Structures of Irosustat metabolites formed *in vitro*, and proposed enzymatic pathways in humans.

DMD Fast Forward. Published on April 4, 2011 as DOI: 10.1124/dmd.111.038315
This article has not been copyedited and formatted. The final version may differ from this version.
DMD #38315

Table 1. Formation of phase I metabolites in the incubations of ^{14}C-Irosustat with liver microsomes from rat, dog, monkey and human (males and females separately) after 120 minutes of incubation. Results are expressed as relative percentage of ^{14}C-labelled metabolites from duplicate incubations.

Metabolite	Relative Percentage of Peak Area in Radio-HPLC Profiles							
	Rat		Dog		Monkey		Human	
	Male	Female	Male	Female	Male	Female	Male	Female
P-14	nd	nd	2.1	0.5	1.3	2.3	nd	nd
M7	**4.5**	**3.7**	**14.7**	**8.1**	**48.5**	**58.8**	**10.1**	**10.4**
M8	**2.2**	**1.3**	**4.9**	**2.8**	**23.1**	**25.0**	**5.0**	**4.2**
M9	0.6	0.4	1.4	1.0	4.4	1.3	2.4	1.6
M10	0.5	1.0	0.5	0.3	2.5	0.6	1.6	1.1
M11	0.9	2.0	nd	nd	nd	nd	0.7	0.9
P-23	nd	nd	0.5	0.7	nd	nd	0.3	0.4
P-24	0.4	nd	1.0	0.7	1.8	1.1	0.4	1.0
M13	**3.8**	**3.7**	**6.5**	**6.1**	**9.9**	**6.9**	**9.5**	**10.9**
M14	**2.9**	**1.6**	**4.6**	**5.5**	**1.1**	**nd**	**2.5**	**2.5**
M15	2.1	1.3	1.6	1.3	nd	nd	0.4	0.8
M16	**5.4**	**4.2**	**7.2**	**7.4**	**5.0**	**3.3**	**8.1**	**9.1**
M18	0.5	0.4	0.7	0.5	*	*	3.2	3.3
^{14}C-Irosustat	**58.7**	**59.2**	**35.5**	**44.8**	**2.4**	**0.7**	**44.6**	**43.3**
P-36	nd	0.6	0.9	0.7	nd	nd	1.6	1.4
667-Coumarin	**17.4**	**20.8**	**18.0**	**19.6**	*****	*****	**9.8**	**9.3**

nd: Peak not detected.

** Peak detected in samples corresponding to intermediate incubation periods.*

Bold: Main metabolites (which accounted for more than 5 % of relative percentage in some species).

DMD Fast Forward. Published on April 4, 2011 as DOI: 10.1124/dmd.111.038315
This article has not been copyedited and formatted. The final version may differ from this version.

Table 2. Comparison of the apparent intrinsic clearance and the percentage of 667-Coumarin formed after 120 minutes in control incubations without cofactor or without liver microsomes. Results are the mean values of duplicate incubations for each batch of HLM.

Liver Microsomes		$\mathbf{Cl_{int,app}}$	**Formation of 667-Coumarin (Relative %)**	
Species	**Sex**	**(ml/min/kg)**	**Without β-NADP**	**Without Microsomes**
Rat	Male	4.3	43.3	36.5
	Female	3.3	47.3	39.1
Dog	Male	3.5	47.7	38.4
	Female	2.3	47.3	39.0
Monkey	Male	23.4	45.4	37.7
	Female	61.5	46.3	40.0
Human	Male	2.3	41.9	37.4
	Female	2.4	42.2	37.7

DMD Fast Forward. Published on April 4, 2011 as DOI: 10.1124/dmd.111.038315
This article has not been copyedited and formatted. The final version may differ from this version.
DMD #38315

Table 3. Correlation between Irosustat metabolite formation in a panel of HLM from 16 different individual donors, and specific activities of individual CYP enzymes and FMO. Results are expressed as the Pearson Correlation Coefficient from the mean of duplicate incubations for each batch of HLM.

Enzymes*	Pearson Correlation Coefficient (r)								
	M7	**M8**	**M9**	**M11**	**M13**	**M14**	**M16**	**M18**	**P-36**
CYP1A2[1]	0.3442	0.2113	0.1063	-0.2011	0.1428	0.1566	0.1633	0.2141	0.1036
CYP1A2[2]	0.3448	0.1842	0.1877	-0.0852	0.2512	0.3685	0.2702	0.1743	0.1871
CYP2A6	0.1461	0.1888	0.3843	0.2659	0.4432	0.4054	0.5487	0.4000	0.5040
CYP2B6[3]	0.0842	0.0561	0.4763	0.4781	0.4743	0.5963	0.6118	0.2896	0.5014
CYP2B6[4]	-0.2274	-0.2807	0.0828	0.3068	0.0793	0.2639	0.2399	-0.0511	0.3690
CYP2C8	0.5678	0.5420	**0.7748*****	**0.6891****	**0.6812****	**0.6607****	**0.7612*****	0.4732	0.5552
CYP2C9	**0.8845*****	**0.8734*****	**0.7457*****	0.2617	**0.7894*****	0.4010	**0.6400****	**0.8397*****	0.5381
CYP2C19	**0.7253****	**0.7077****	0.5973	-0.0048	**0.7237****	0.4801	**0.6592****	**0.8776*****	0.5918
CYP2D6	-0.1915	-0.0889	0.0417	-0.0502	0.1044	0.3233	0.1177	-0.0034	-0.3070
CYP2E1	**0.6430****	0.4251	0.5158	0.3324	0.3751	0.2590	0.3077	0.2424	0.3554
CYP3A4/5[5]	0.2255	0.2284	0.5628	0.1269	**0.6830****	**0.9490*****	**0.7338****	0.3922	0.3699
CYP3A4/5[6]	0.2009	0.1563	0.5147	0.1804	**0.6452****	**0.9273*****	**0.7051****	0.2731	0.4055
FMO3	-0.2383	-0.1785	-0.3982	-0.4268	-0.3530	-0.2174	-0.3755	-0.2916	-0.3942

**Enzyme activities: 7-ethoxyresorufin O-dealkylation[1] and phenacetin O-deethylation[2] (for CYP1A2), coumarin 7-hydroxylation (for CYP2A6), S-mephenytoin N-demethylation[3] and bupropion hydroxylation[4] (for CYP2B6), paclitaxel 6α-hydroxylation (for CYP2C8), diclofenac 4'-hydroxylation (for CYP2C9), S-mephenytoin 4'-hydroxylation (for CYP2C19), dextromethorphan O-demethylation (for CYP2D6), chlorzoxazone 6-hydroxylation (for CYP2E1), testosterone 6β-hydroxylation[5] and midazolam 1'-hydroxylation[6] (for CYP3A4/5), and benzydamine N-oxidation (for FMO)*

** *Statistically significant correlation ($p < 0.01$)*

*** *Statistically significant correlation ($p < 0.001$)*

DMD Fast Forward. Published on April 4, 2011 as DOI: 10.1124/dmd.111.038315
This article has not been copyedited and formatted. The final version may differ from this version.
DMD #38315

Table 4. Inhibition of the formation of Irosustat metabolites in incubations with HLM in the presence of CYP-selective chemical inhibitors. Results are expressed as percentage of inhibition relative to control incubations (without inhibitor), and are the mean values from duplicate incubations except for CYP2C19 which were triplicate incubations.

Chemical Inhibitors**	**Inhibition %**								
	M7	**M8**	**M9**	**M11**	**M13**	**M14**	**M16**	**M18**	**P-36**
CYP1A2	-1.9	-1.4	0.0	-22.2	-0.2	14.4	-16.1	-4.4	-4.5
CYP2A6	**45.6***	**48.0***	**22.1***	5.0	nq	nq	**32.9***	**53.0***	**37.1***
CYP2B6	**23.5***	**21.4***	**47.9***	**48.1***	**30.2***	**32.0***	**24.1***	**30.3***	17.7
CYP2C8	**51.5***	**49.4***	**64.9***	**50.0***	**50.9***	**33.4***	**43.3***	**61.4***	**35.8***
CYP2C9	**41.8***	**71.2***	17.7	8.9	**51.3***	-1.5	**37.7***	**65.7***	**60.5***
CYP2C19[a]	10,0	19,6	13,8	17,3	14,0	-24,8	9,4	19,8	10,9
CYP2C19[b]	-2,8	-9,3	-18,4	-17,0	-4,8	-21,2	-9,0	1,3	-3,5
CYP2D6	14.5	nq	nq	nq	12.6	10.7	8.4	**22.6***	6.9
CYP2E1	**24.3***	4.5	17.5	**33.6***	9.9	4.7	7.5	**26.9***	8.8
CYP3A4/5	11.8	1.0	**36.5***	15.3	**24.0***	**55.7***	**20.3***	**23.5***	-4.1

** Percentage of Inhibition >20%*

*** CYP Inhibitors: 1 µM furafylline (CYP1A2); 0.1µM methoxsalen (CYP2A6); 750 µM orphenadrine (CYP2B6); 10 µM quercetin (CYP2C8); 2 µM sulfaphenazole (CYP2C9); 100 µM nootkatone[a], and 5 µM (+)-N-3-benzyl-nirvanol[b] (CYP2C19); 0.5 µM quinidine (CYP2D6);15 µM 4-methylpyrazole (CYP2E1); and 0.5 µM ketoconazole (CYP3A4/5).*

nq: not quantified due to HPLC coelution of the inhibitor with the metabolites.

DMD Fast Forward. Published on April 4, 2011 as DOI: 10.1124/dmd.111.038315
This article has not been copyedited and formatted. The final version may differ from this version.

Table 5. Formation of Irosustat metabolites in incubations with human cDNA-expressed CYPs and FMO3 enzyme. Results are expressed as mean of metabolite peak area units from duplicate incubations.

Enzyme	Mean Peak Area								
	M7	**M8**	**M9**	**M11**	**M13**	**M14**	**M16**	**M18**	**P-36**
CYP1A1	3784	nd	nd	nd	25693	30242	30049	3196	nd
CYP1A2	39779	8781	15849	nd	105131	69618	37042	16618	nd
CYP1B1	nd	nd	nd	nd	4978	nd	15681	nd	nd
CYP2A6	nd	nd	nd	nd	nd	nd	nd	nd	nd
CYP2B6	nd	nd	nd	nd	nd	nd	3132	nd	5565
CYP2C8	nd	nd	2653	nd	2731	nd	nd	nd	nd
CYP2C9	4129	nd	nd	nd	4904	nd	2106	2648	nd
CYP2C19	15105	4528	2444	nd	22693	nd	14730	6638	8235
CYP2D6	125154	20891	3785	nd	52889	nd	12864	4213	nd
CYP2E1	10210	1923	nd	nd	2599	nd	nd	nd	nd
CYP3A4	nd	nd	7425	nd	88686	51656	26628	5335	nd
CYP3A5	1855	nd	2159	nd	12175	1915	4855	2915	nd
FMO3	nd	nd	nd	nd	nd	nd	nd	nd	nd

nd: not detected

DMD Fast Forward. Published on April 4, 2011 as DOI: 10.1124/dmd.111.038315
This article has not been copyedited and formatted. The final version may differ from this version.
DMD #38315

Table 6. Investigation of the role of CYP1A2 in Irosustat metabolism. Formation of Irosustat metabolites in incubations with native and CYP1A2-fortified HLM. Results are expressed as percentage of inhibition for each separate metabolite, and are the mean values from duplicate incubations.

Matrix	Chemical Inhibitors	Inhibition %								
		M7	**M8**	**M9**	**M11**	**M13**	**M14**	**M16**	**M18**	**P-36**
Native HLM	**FU**	1.4	2.0	4.3	*-59.5*	1.7	2.7	1.2	2.4	1.9
	MIX	**66.2**	**100**	**74.6**	**100**	**65.0**	**49.5**	**70.3**	**64.4**	**47.7**
	MIX + FU	**65.6**	**100**	**81.3**	**100**	**66.5**	**54.6**	**81.3**	**68.0**	**54.6**
CYP1A2-fortified HLM	**FU**	-2.6	-8.2	-0.3	*-15.0*	7.0	**24.9**	12.1	0.8	-17.1
	MIX	**44.7**	**44.7**	**58.2**	**100**	**44.3**	**23.7**	**29.6**	**46.1**	**22.6**
	MIX + FU	**56.3**	**61.5**	**72.9**	**100**	**61.1**	**54.2**	**53.8**	**60.7**	**32.8**

FU : 1 µM furafylline

MIX: 10 µM quercetin + 2 µM sulfaphenazole + 20 µM tranylcypromine + 0.5 µM ketoconazole

Microsomal protein concentration: 1 mg/ml ± 20 pmol/ml recombinant human CYP1A2

Incubation time: 15 min preincubation ± furafylline followed by 40 min incubation

Irosustat concentration: 50 µM

Bold numbers: percentage of inhibition > 20%

Cursive values: high variability for M11 since peak areas were close the limit of detection

DMD Fast Forward. Published on April 4, 2011 as DOI: 10.1124/dmd.111.038315
This article has not been copyedited and formatted. The final version may differ from this version.
DMD #38315

Table 7. Formation of Irosustat metabolites in incubations with human cDNA-expressed UGT enzymes. Results are expressed as mean of metabolite peak area units from duplicate incubations.

Enzyme	Mean Peak Area								
	G1*	**G2***	**G3***	**G4***	**M2**	**M4***	**G7***	**G8***	**M12****
UGT1A1	3426	4859	nd	nd	9573	3341	nd	nd	451831
UGT1A3	nd	nd	nd	nd	31109	11989	nd	nd	521544
UGT1A4	nd	nd	nd	nd	nd	nd	nd	nd	nd
UGT1A6	nd	nd	nd	nd	nd	nd	nd	nd	15031
UGT1A7	nd	nd	nd	nd	3228	nd	nd	nd	68845
UGT1A8	nd	nd	nd	nd	7468	2584	nd	5038	330741
UGT1A9	nd	4860	6819	nd	11240	3141	nd	25835	228401
UGT1A10	nd	nd	nd	nd	nd	nd	nd	nd	86036
UGT2B4	nd	nd	nd	nd	3619	nd	nd	nd	210011
UGT2B7	nd	nd	nd	nd	6706	nd	nd	nd	510503
UGT2B15	nd	nd	nd	3135	24520	4696	nd	nd	541538
UGT2B17	nd	nd	nd	nd	nd	nd	12861	nd	320705

nd: not detected

** : Unidentified glucuronide conjugates*

*M12**: Incubations performed with 667-Coumarin*

DMD Fast Forward. Published on April 4, 2011 as DOI: 10.1124/dmd.111.038315
This article has not been copyedited and formatted. The final version may differ from this version.

Table 8. Formation of Irosustat metabolites in incubations with human cDNA-expressed SULT enzymes. Results are expressed as mean of metabolite peak area units from duplicate incubations.

Enzyme	Mean Peak Area							
	M3	**S2***	**S3***	**S4***	**S5***	**S6***	**M17****	**S7***
SULT 1A1*1	12626	12773	2645	4299	6554	9783	99619	3040
SULT 1A1*2	4672	3753	nd	2521	nd	6892	59468	2835
SULT 1A2*1	2604	nd	nd	nd	nd	nd	17799	2802
SULT 1A3	nd	nd	nd	nd	nd	4066	nd	3950

nd: not detected

** : Unidentified sulphate conjugates*

*M17**: Incubations performed with 667-Coumarin*

Fig. 1

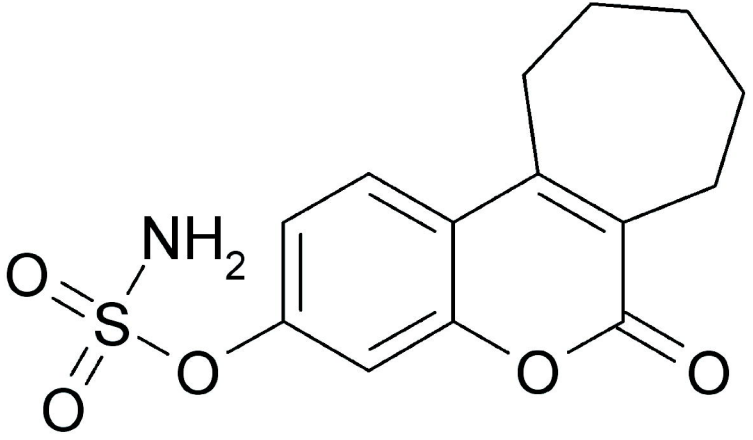

A

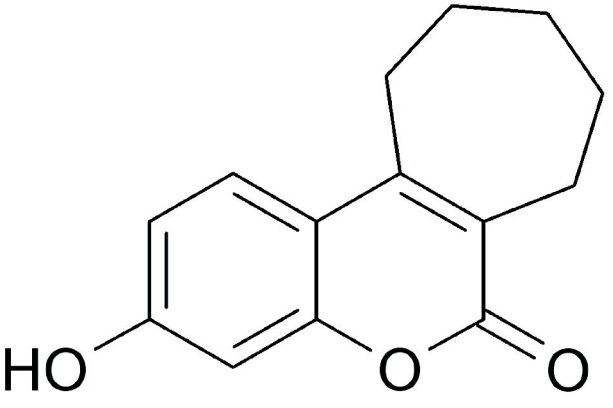

B

Fig. 2

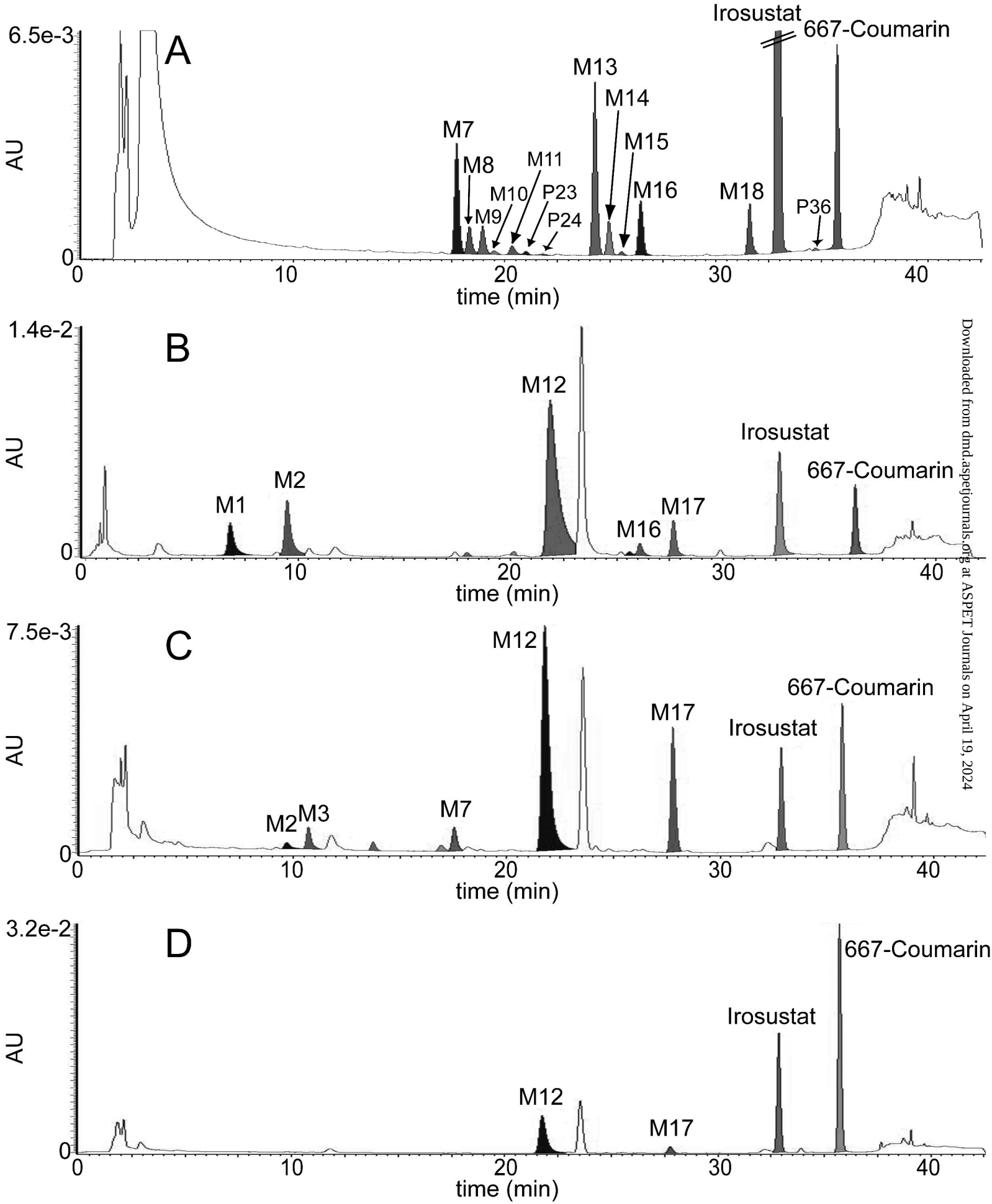

Fig. 3

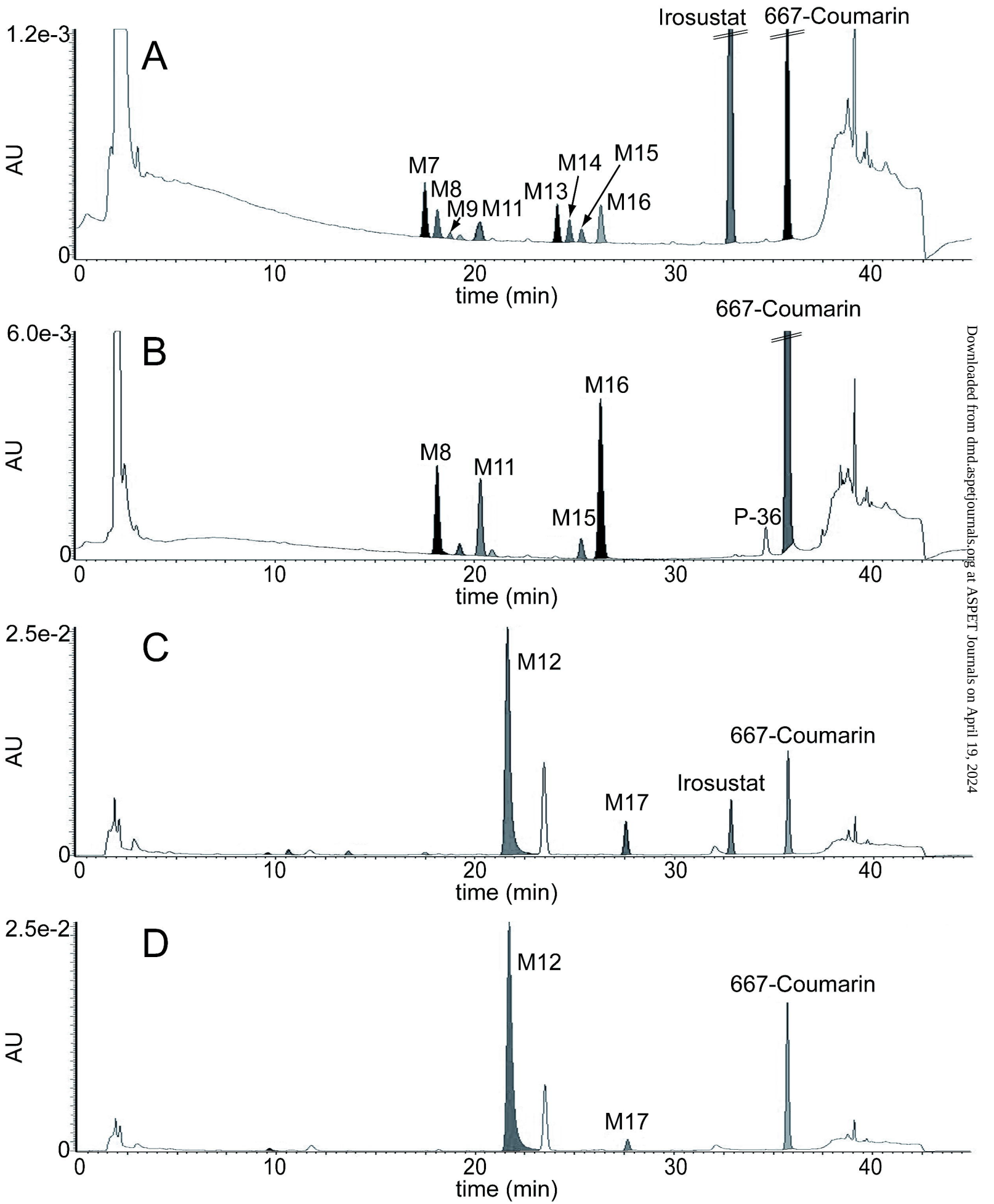

Fig. 4

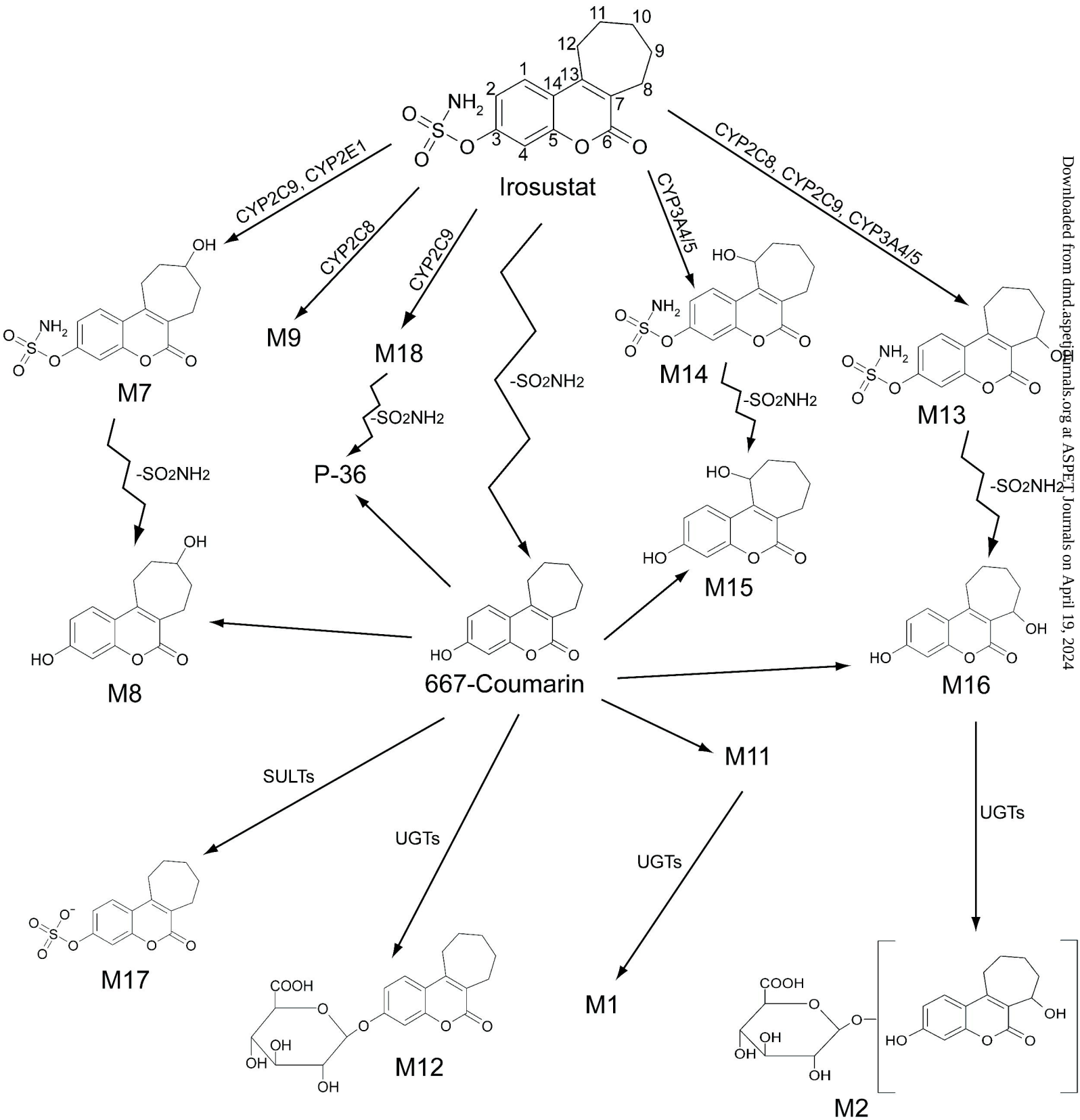

Supplemental Data 1

Verònica Ventura, Josep Solà, Carles Celma, Concepción Peraire and Rosendo Obach.

In Vitro Metabolism of Irosustat, a Novel Steroid Sulphatase Inhibitor: Inter-Species Comparison, Metabolite Identification and Metabolic Enzyme Identification.

Drug Metabolism and Disposition (DMD #38315)

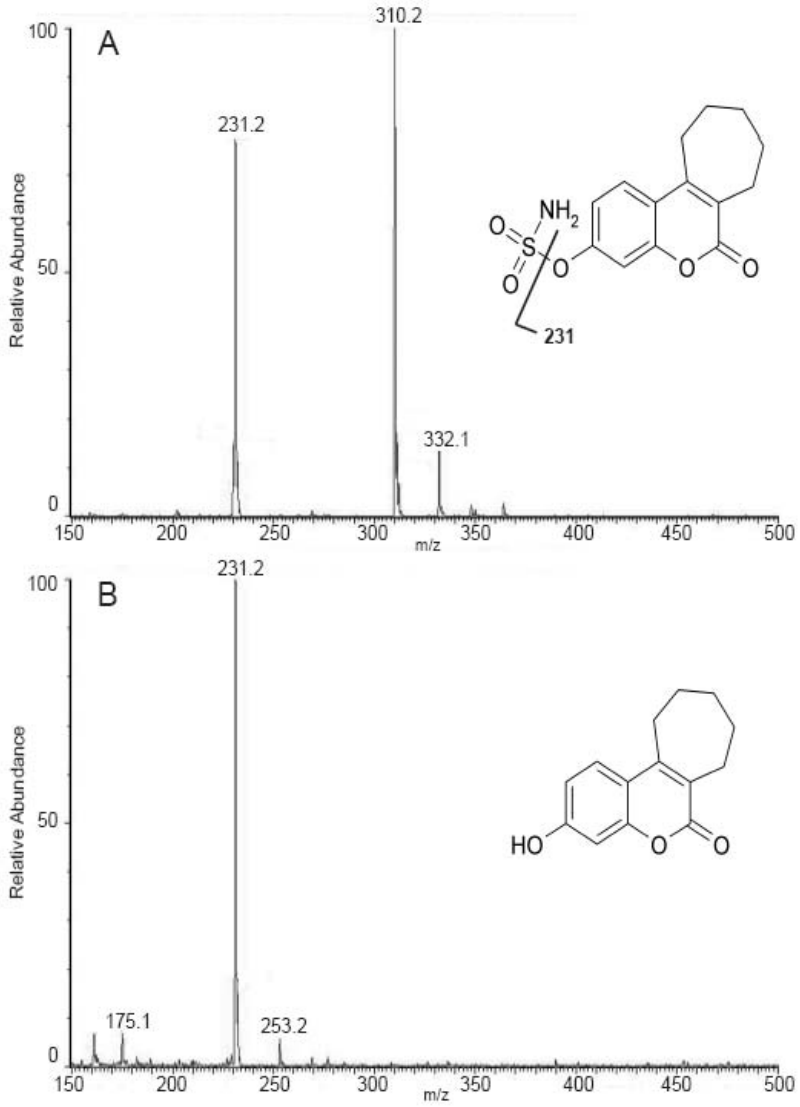

Fig. 1. MS Spectra (ESI positive ion mode) of Irosustat (A) and 667-Coumarin (B) at 60 V cone voltage.

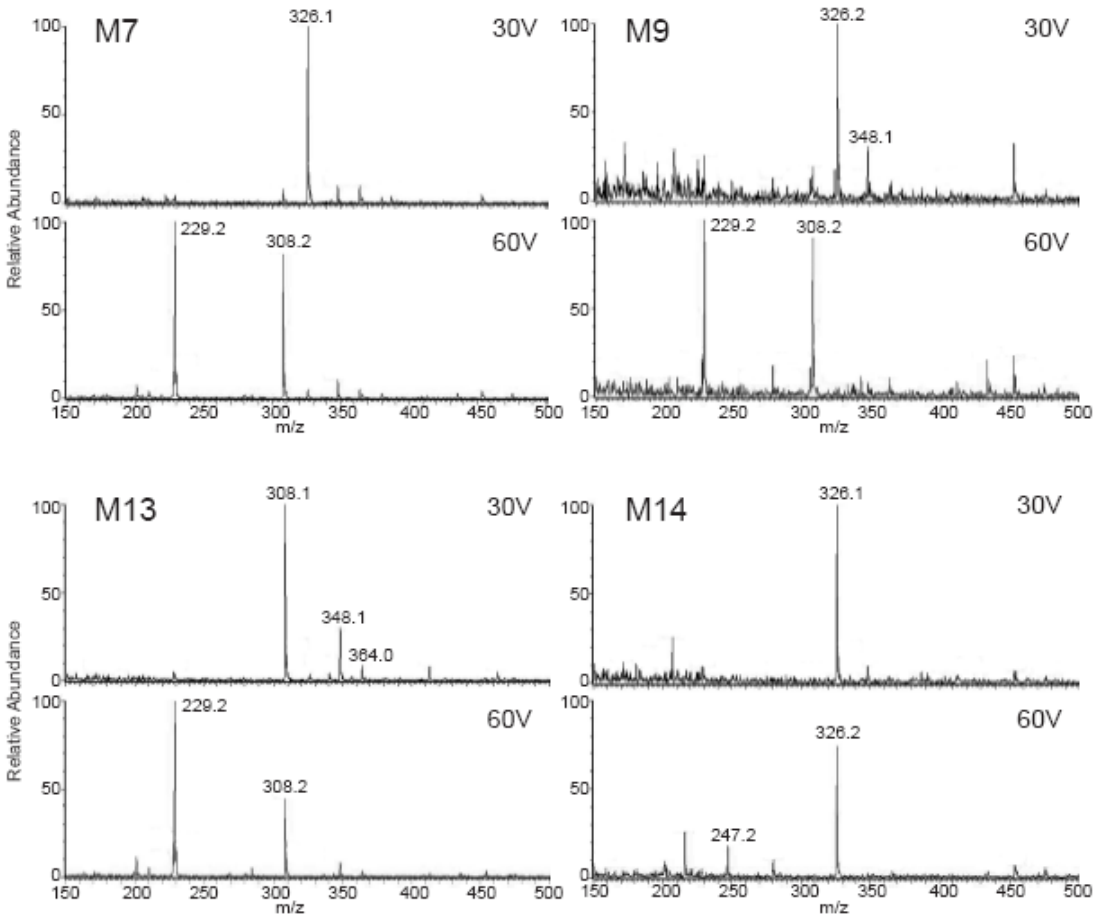

Fig. 2. MS Spectra (ESI positive ion mode) of the mono-oxidized metabolites of Irosustat: M7, M9, M13 and M14. Upper panel: MS spectra obtained at 30 V cone voltage; Lower panel: MS spectra obtained at 60 V cone voltage. M7, M9 and M14 showed a protonated molecular ion of *m/z* 326, representing an increase of 16 mass units in its parent compound Irosustat. Although M13 showed a protonated molecular ion of *m/z* 308, the formation of ions showing *m/z* consistent with the Na^+ and K^+ adducts of *m/z* 326, suggested that M13 was also a mono-oxidized metabolite of Irosustat, and that probably was dehydrated in the MS source (consequently losing 18 mass units).

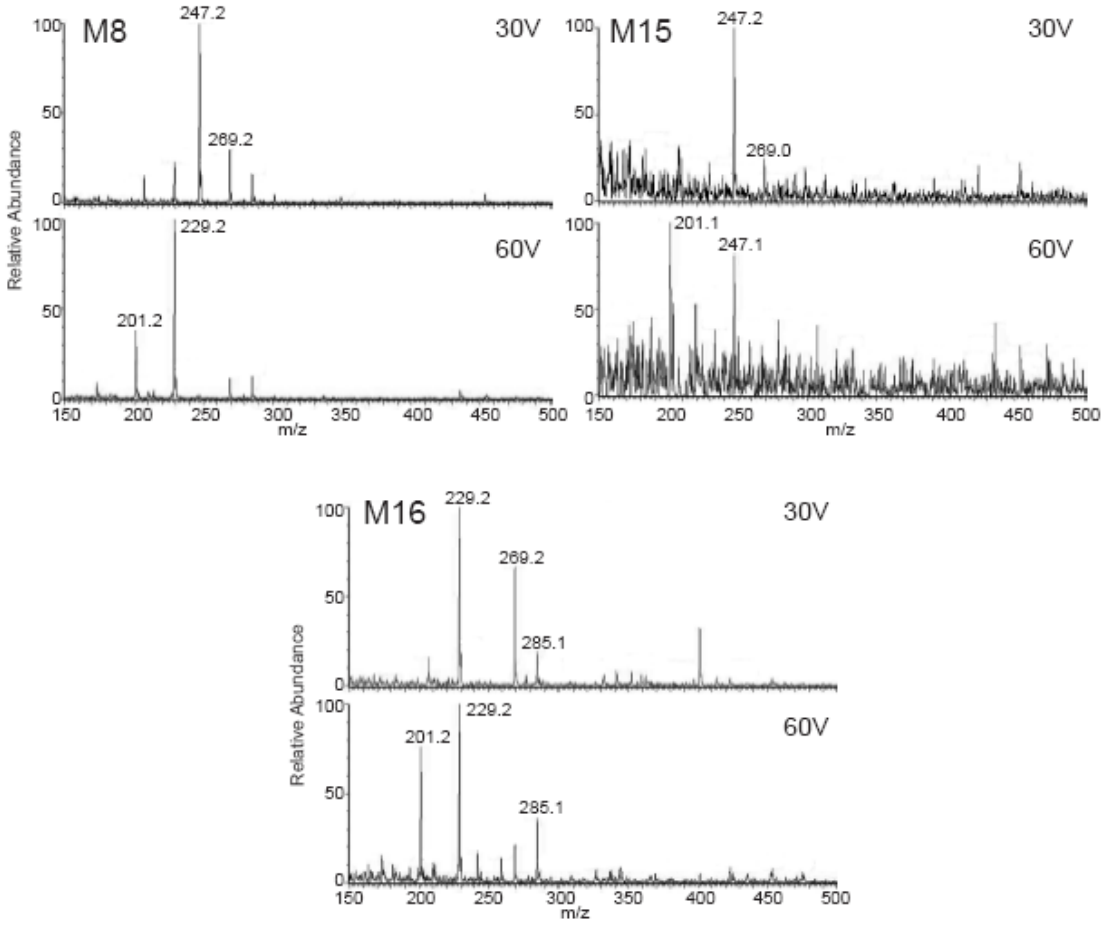

Fig. 3. MS Spectra (ESI positive ion mode) of the mono-oxidized metabolites of 667-Coumarin: M8, M15 and M16. Upper panel: MS spectra obtained at 30 V cone voltage; Lower panel: MS spectra obtained at 60 V cone voltage. M8 and M15 showed a protonated molecular ion of *m/z* 247, representing an increase of 16 mass units in its parent compound 667-Coumarin. Although M16 showed a protonated molecular ion of *m/z* 229, the formation of ions showing *m/z* consistent with the Na^+ and K^+ adducts of *m/z* 247, suggested that M16 was also a mono-oxidized metabolite of 667-Coumarin, and that probably was dehydrated in the MS source (consequently losing 18 mass units).

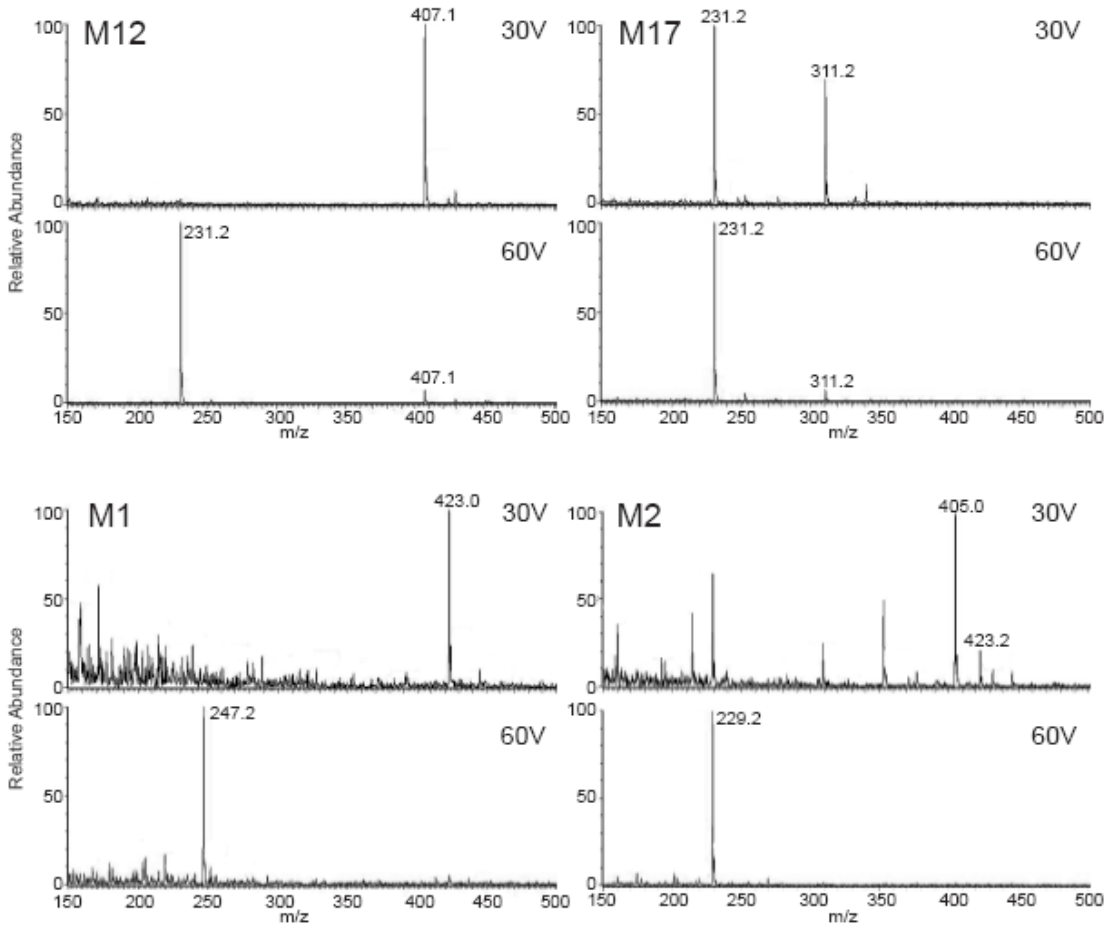

Fig. 4. MS Spectra (ESI positive ion mode) of the 667-Coumarin glucuronide: M12; the 667-Coumarin sulphate: M17; and two glucuronides of mono-oxidized 667-Coumarin metabolites: M1 (glucuronide of metabolite M11), and M2 (glucuronide of metabolite M16). Upper panel: MS spectra obtained at 30 V cone voltage; Lower panel: MS spectra obtained at 60 V cone voltage. At the cone voltage of 60 V, M1 showed a fragmentation product of *m/z* 247 corresponding to the mono-oxidized 667-Coumarin residue after the neutral loss of the glucuronide, whereas M2 showed a fragmentation product of *m/z* 229 corresponding to a typical fragmentation product of some mono-oxidized 667-Coumarin derivatives. Metabolites M12 and M17 showed a fragmentation product of *m/z* 231 corresponding to the *m/z* of 667-Coumarin residue after the neutral loss of the glucuronide or the sulphate, respectively.